Voltage Calibration of the Direct Electrooptic Sampling Technique

Dag R. Hjelme and Alan R. Mickelson

Abstract—**A detailed study of various voltage calibration factors for the direct electrooptic sampling technique is presented. In reflection mode optical probing, the circuit substrate forms an etalon for the optical probe beam. Analytical expressions for the calibration factors due to etalon effects and decaying surface potentials are derived. Depending on the length of the sampling pulse relative to the substrate transit time, the etalon will affect either the voltage calibration factor or the system bandwidth. For pulses long compared to the transit time, interference at the surface results in a probe wavelength dependent storage time effect. The resulting electrooptic signal shows a resonant behavior as a function of wavelength or substrate thickness. For pulses short compared to the substrate transit time, multiple reflections reduce the effective system bandwidth to a bandwidth less than that given by the single transit time or the sampling pulse width. Experimental verification of the theoretical results are presented. Various deembedding procedures for implementing the voltage calibration are discussed.**

I. Introduction

THE CONTINUED increase in the operating frequency of monolithic microwave integrated circuits (MMICs) as well as other very high speed electronics devices have necessitated a need for new instrumentation and measurement techniques. With the objective of high-frequency, noninvasive probing of internal signals in MMICs, a number of new measurement techniques, including various optical sampling techniques, have been developed for these applications. In particular the electrooptic sampling technique has shown promising results, and been the focus of intense development the last few years [1]–[4].

Although the electrooptic sampling technique has been successfully used for a variety of circuit characterization problems [5], [6], little attention has been focused on the accuracy of the technique. As in conventional (electrical) contact probing techniques, the probe geometry and system hardware can introduce significant measurement errors that must be removed if accurate measurements are to be made. In conventional probing significant errors are introduced due to discontinuities in probes and connectors. In the past, efforts were made to minimize the errors by designing more perfect hardware items. However, it is now recognized and accepted that one can correct for these errors rather than try to eliminate them completely. In modern network analyzers system error calibration and corrections provide high accuracy and reduced system cost. A procedure referred to as deembedding has been developed to implement the calibration [7].

Direct electrooptic probing relies on the circuit substrate to be a part of the measurement system. Accordingly, the electrooptic interactions in the substrate must be investigated in detail to design deembedding procedures and implement the calibration of the direct electrooptic sampling technique. To the best of our knowledge, no detailed discussion of these calibration issues has been presented in the literature. The most important effects are the multiple reflections of the probe pulse in the substrate. Li *et al.* [8] have recently observed interferometric effects in the electrooptic signal from microstrip devices. They pointed out the resulting calibration difficulties, but did not discuss any possible calibration procedures. Other possible measurement errors of the direct electrooptic sampling technique, that must be corrected for in a calibration procedure, are reduced sensitivity due to the rapidly decaying surface potential away from the signal line in microstrip circuits, and cross-talk due to fringing fields from neighboring lines in coplanar transmission line circuits. Using numerical techniques to calculate the fringing microwave fields these effects have been studied by various groups [9], [10], [11], [6]. To efficiently correct for these effects simple analytical formulas for the correction factors are needed. No such analytical correction factors have been reported. These effects due to fringing fields are analogous to the cross-talk due to probe proximity in conventional contact probing techniques.

In this paper we will present both theoretical and experimental results on various calibration issues important for the electrooptic probing technique. Specifically, we will present calibration factors resulting from the inherent substrate etalon in the direct electrooptic probing technique. Interferometric effects in the long pulse limit will be shown to lead to a strong probe wavelength or substrate thickness dependent voltage calibration factor, while the multiple reflection in the short pulse limit will lead to fre-

Manuscript received March 6, 1991; revised March 20, 1992. This work was supported by the NSF Industry/University Cooperative Research Center for Microwave/Millimeter Wave Computer Aided Design under grant No. CDR-8722832, and by the Office of Naval Research under grant No. ONRN00014-92-J-1190.

The authors are with the Department of Electrical and Computer Engineering University of Colorado, Campus Box 425, Boulder, CO 80309-0425.

IEEE Log Number 9202141.

quency dependent amplitude and phase calibration factors. The second issue to be discussed is the geometrical calibration factor in microstrip circuits. Voltage calibration factors due to probe beam spot size and location will be presented. Furthermore, based on the presented models, we will discuss various possible deembedding procedures that can be used to remove the measurement errors introduced by substrate variations.

The paper is organized as follows. In Section II we present a theoretical analysis of etalon effects in an electrooptic sampling set-up. First, in Section II-A, we present a review of the analysis of the electrooptic sampling set-up ignoring substrate etalon effects. Next, in Section II-B we present a general analysis of the set-up including etalon effects. The resulting expression for the receiver signal is valid for any combination of probe pulse and substrate etalon. This general result is then analyzed in detail for two limiting cases. In Section II-C we present the results for sampling pulses long compared to the substrate transit time, while in Section II-D we discuss the case of very short pulses. Next, in Section II-E, we derive expressions for the geometrical calibration factors in microstrip circuits. In Section III, we present experimental results of the etalon effect in a GaAs MMIC amplifier using a Nd:YAG laser and a tunable dye-laser. Next, in Section IV we discuss possible applications of the theoretical model to the development of a deembedding algorithm to remove the measurement errors from the data. Finally, in Section V, we discuss the results and conclude.

II. Theory

A. The Electrooptic Sampling System

In the direct electrooptic sampling technique the microwave field induced birefringence changes the probe beam state of polarization, this in turn is converted to amplitude modulation in a polarizing beam splitter. The resulting amplitude modulation is directly proportional to the integral of the field induced phase perturbation along the optical path, and therefore proportional to the circuit voltage. Some commonly used probing geometries are shown in Fig. 1. In Fig. 1(a) and (b), the probe beam is reflected off the ground plane or signal lines, forming an asymmetric Fabry–Perot etalon. The geometry shown in Fig. 1(c) forms a symmetric Fabry–Perot etalon for the probe beam. In all cases the resulting etalon reflection coefficients will have frequency dependent magnitude and phase. If the backside reflectivity is one, the resulting etalon is purely dispersive (Gires–Tournois etalon [12]).

The two standard set-ups used for reflection-mode probing in GaAs are shown in Fig. 2. With obvious modifications, the set-ups can be used with substrates with crystal symmetries different from GaAs. In both set-ups polarization optics are used to set the static retardation of the system to $\pi/2$ to bias the electrooptic modulator at the quarter wave point, and to maximize the linear modulation range. In Fig. 2(a), the linear input polarization is transformed to an elliptic polarization with major axis oriented at 45° entering the substrate. On the return, the elliptic polarization is transformed to a linear polarization at 45° entering the polarizing beam splitter. In Fig. 2(b) the linear input polarization is transformed to a circular polarization entering the substrate and the output polarizing beam splitter is oriented at 45°. The additional losses in the non-polarizing beamsplitter can be avoided by using a slightly angled input beam and a mirror to deflect the beam to the polarizing beamsplitter. Any electrooptically induced birefringence in the substrate causes the reflected polarization to deviate from the incident polarization state resulting in an amplitude modulation at the detector. In this paper we will, for simplicity, restrict our analysis to the system in Fig. 2(b). Since both set-ups are biased at the quarter-wave point and use equal intensities in the x- and y-polarizations incident on the substrate, they are identical from a system point of view.

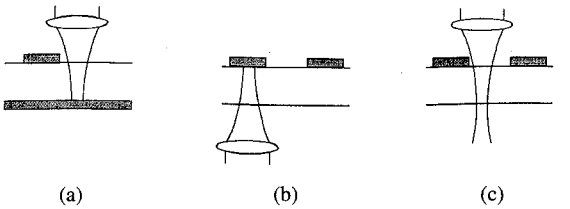

Fig. 1. Some commonly used probing geometries. (a) Front-side probing for a microstrip line. (b) Back-side probing for a coplanar stripline. (c) Front-side probing for a coplanar stripline.

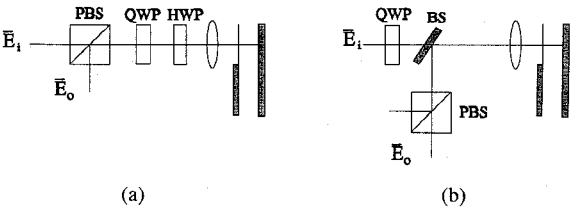

Fig. 2. Electrooptic sampling head arrangements for separation of incident and reflected beams in reflection-mode probing. (a) Arrangement using a polarizing beam splitter (PBS), a quarter-wave plate (QWP) oriented at $\pi/8$, and a half-wave plate (HWP) oriented at $3\pi/16$. (b) Arrangement using a quarter-wave plate (QWP) to generate a circularly polarized probe beam, and using a non-polarizing beam splitter (BS) to direct the beam through a polarizing beamsplitter (PBS) oriented at $\pi/4$.

To keep the analysis transparent it is convenient to represent the reflection off the circuit substrate by two reflection operators, defined through the relations

$$E_j^{(r)}(t) = \hat{r}_j(V(t))E_j^{(i)}(t), \qquad j = x, y \tag{1}$$

where the superscripts (r) and (i) denotes the reflected and incident fields, x and y represents two crystal axes ([110] and [$\bar{1}$10] direction in GaAs), and $V(t)$ is the applied microwave voltage. Using Jones matrices, the output electric field vectors in the set-up shown in Fig. 2(b) can then be written as

$$\vec{E}_o(t) = \frac{1}{2}\begin{bmatrix} 1 & 1 \\ 1 & 1 \end{bmatrix}\begin{bmatrix} \hat{r}_x(V(t)) & 0 \\ 0 & \hat{r}_y(V(t)) \end{bmatrix}\frac{1}{\sqrt{2}} \cdot \begin{bmatrix} 1 & -i \\ -i & 1 \end{bmatrix}\vec{E}_i(t) \tag{2}$$

where $\vec{E}_t(t)$ is the input electric field vector. The three matrices in (2) represent, from left to right, the polarizing beamsplitter rotated to 45°, the circuit substrate, and the quarter wave plate. Using a slow photodetector, the receiver signal will be proportional to the time averaged output intensity $\langle I_o(t)\rangle = \langle|\vec{E}_o(t)|^2\rangle$, where the angular brackets denote a time average with the averaging time long compared to the laser pulse train repetition rate, but short compared to the IF signal period. Assuming the input field vector is linearly polarized along the x-axis, $\vec{E}_i(t) = E(t)\,\vec{x}$, the output field vector immediately follows from (2). Performing the matrix multiplication, taking the magnitude squared, and applying the time averaging we find

$$\langle I_o(t)\rangle = \langle|\vec{E}_o(t)|^2\rangle = \langle|\tfrac{1}{2}\{\hat{r}_x(V(t)) - i\hat{r}_y(V(t))\}E(t)|^2\rangle \tag{3}$$

where $E(t)$ is the input laser pulse train. Equation (3) is completely general. Once expressions for the reflection operators are given, the receiver signal can be calculated. However, before we evaluate the receiver signal including substrate etalon effects, it is useful to consider the standard analysis where surface reflections are neglected.

In the standard analysis of the electrooptic sampling system the reflection from the front surface is neglected, and the backside reflectivity is set to one. Furthermore, the time variation of the microwave field in one substrate transit time is ignored. For a substrate thickness of h the reflection operator takes the simple form

$$\hat{r}_j(V(t)) = e^{-i[\phi_0 + \phi_j(V(t))]}, \qquad j = x, y \tag{4}$$

where $\phi_0 = 2kh$ is the round trip phase delay of the substrate, and $\phi_j(V(t))$ is the microwave field induced phase shift. For small induced phase shifts ($|\phi_y - \phi_x| \ll \pi/2$), the time averaged intensity now follows from (3) and (4) as

$$\langle I_o(t)\rangle = \tfrac{1}{2}\{\langle I(t)\rangle - \langle(\phi_y - \phi_x)I(t)\rangle\} \tag{5}$$

where $I(t) = |E(t)|^2$ is the laser pulse train intensity. For GaAs substrate, we have $\phi_y = -\phi_x \equiv \pi V/V_\pi$, where $V_\pi = \lambda_0/(2n_0^3 r_{14})$ is the halfwave voltage, and r_{14} is the electrooptic coefficient. The microwave field induced phase difference can then be written

$$\phi_y - \phi_x = \frac{2\pi V}{V_\pi} \tag{6}$$

With sufficient short laser pulses $I(t)$, the sampling signal will be linearly proportional to the applied voltage $V(t)$ normalized to V_π. If the assumptions of negligible surface reflection and unity backside reflection coefficient were true, the only calibration factor would be the half wave voltage.

For the case of cw microwave field excitation, $V(t) = \mathrm{Re}\{\hat{V}\exp(i(\omega_m t + \phi_V))\}$, it is convenient to express the laser pulse train as

$$I(t) = \mathrm{Re}\left\{\sum_{n=0}^{\infty} I_n e^{in\omega_L t}\right\}. \tag{7}$$

After time averaging, only the pulse harmonic closest to the microwave frequency ω_m will contribute to the receiver signal at the IF frequency. Assuming the Nth pulse harmonic is closest to the microwave frequency, the IF frequency is defined as $\Delta\omega \equiv \omega_m - N\omega_L$. If the laser pulse width is much shorter than the inverse of the applied microwave frequency we have $I_N \approx I_o = \langle I(t)\rangle$. The time averaged intensity can now be written

$$\langle I_o(t)\rangle = \frac{1}{2}\langle I(t)\rangle\left\{1 - \frac{2\pi}{V_\pi}|\hat{V}|\cos(\Delta\omega t + \phi_V)\right\}. \tag{8}$$

B. Pulse Propagation in a Time Varying Etalon

The probe pulse propagation in the substrate can be described by the field envelope equation [13]

$$\left[\partial_z - ik + \frac{1}{v_g}\partial_t\right]E(z, t) = i\Delta k(z, t)E(z, t) \tag{9}$$

where $\Delta k(z, t)$ is the local microwave field induced change in the wavenumber k. In general $\Delta k(z, t)$ would be given by the product of a z-dependent part, given by the mode profile of the transmission line mode, and a time dependent function given by the time waveform

$$\Delta k(z, t) = \Delta k_m(z) f(t). \tag{10}$$

An approximate solution of (9), valid for small microwave field induced phase shifts, can be written as

$$E(z, t) \approx \exp\{-ikz - i\phi(t - z/v_g)\}E(0, t - z/v_g) \tag{11}$$

where we have defined the microwave field induced phase shift

$$\phi(t - z/v_g) \equiv \int_0^z d\zeta\,\Delta k(\zeta, T + \zeta/v_g) \tag{12}$$

and introduced the new coordinates $\zeta = z$ and $T = t - z/v_g$.

Besides a constant factor due to the surface reflection coefficients, the field after one round trip in the substrate is given by $E(2h, t)$. It is convenient to write this in the form

$$E(2h, t) \approx \exp\{-i[\exp(-\tau\,\partial_t)\phi(t) + \hat{\phi}_0]\}E(0, t) \tag{13}$$

where $\tau = 2h/v_g$ is the substrate transit time, $e^{-\tau\partial_t}$ is a time shift operator ($e^{-\tau\partial_t}\phi(t) \equiv \phi(t - \tau)$), $\exp(-i\hat{\phi}_0) \equiv \exp(-i(\phi_0 - i\tau\partial_t))$ is an operator operating on $E(0, t)$ ($\exp(-i\hat{\phi}_0)E(0, t) \equiv \exp(-i\phi_0)E(0, t - \tau)$). It is now straight forward to write an expression for the etalon reflection operator by summing the contributions from the multiple reflections in the substrate

$$\hat{r}_j = -r_f + r_b t_f^2 \sum_{k=0}^{\infty}(r_f r_b)^k \cdot \exp\{-i(k + 1)[\hat{H}_k\phi_j(t) + \hat{\phi}_0]\}, \qquad j = x, y \tag{14}$$

where r_f and t_f are the front surface amplitude reflection and transmission coefficients, r_b is the back surface reflection coefficient. $\hat{H}_k$ is an operator operating on $\phi(t)$ and is defined as

$$\hat{H}_k \equiv \frac{1}{k+1} \sum_{l=0}^{k} (e^{-\tau \partial_t})^{l+1}. \tag{15}$$

As will be demonstrated below, $\hat{H}_k \phi(t)$ describes the multiple transit time effects, and is a generalization of single transit time effect discussed in the literature [1], [2].

Using (14) in (3), we can write the time averaged intensity as

$$\langle I_o(t) \rangle = \tfrac{1}{4} \langle | [-r_f(1-i) + r_b t_f^2 \sum_{k=0}^{\infty} (r_f r_b)^k \cdot \{ e^{-i(k+1)\hat{H}_k \phi_x} - ie^{-i(k+1)\hat{H}_k \phi_y} \} \cdot e^{-i(k+1)\hat{\phi}_0}] E(t) |^2 \rangle. \tag{16}$$

Generally, ϕ_j is caused by either a train of short electrical pulses as would be the case if the circuit is excited from a photoconductive switch, or a sum of a few harmonics of a cw microwave frequency if the circuit is excited from a cw source. The optical probe field $E(t)$ is a train of short laser pulses, which also can be represented as a large number of phaselocked laser modes (see (7)). Therefore, one could represent both $E(t)$ and $\phi_j(t)$ as a series of frequency harmonics making it trivial to apply the operations in (16). However, the general expression for the receiver signal would be in the form of the squared magnitude of an infinite series. Simple analytical results can be obtained in two important cases to be considered in the next two sections.

Before we proceed it is useful to consider the case of sinusoidal excitation ($f(t) = \exp(i\omega_m t)$), and study the effect of $\hat{H}_k$ on the sampling signal. Using (12), (10), and (15) we can write

$$\hat{H}_k \phi(t) = \mathrm{Re} \left\{ g(\omega_m) \frac{\sin((\omega_m(k+1)\tau/2)}{(k+1)\omega_m \tau/2} \cdot e^{-i\omega_m(k+1)\tau/2} \phi_m e^{i\omega_m t} \right\} \tag{17}$$

where

$$g(\omega_m) = \frac{v_g \int_0^{\tau} dt' \Delta k_m(v_g t') e^{i\omega_m t'}}{\phi_m \dfrac{\sin(\omega_m \tau/2)}{\omega_m \tau/2} e^{i\omega_m \tau/2}} \tag{18}$$

and $\phi_m = \tau v_g \Delta k_0$ is the induced phase shift with a uniform microwave field ($\Delta k_m(z) = \Delta k_0$). $g(\omega_m)$ describes the variation of the system frequency response due to a nonuniform microwave field distribution. In reflection mode probing $\Delta k_m(v_g t')$ is always symmetric around $\tau/2$ resulting in a real $g(\omega_m)$. With a uniform field $g(\omega_m) = 1$ and the magnitude of $\hat{H}_k \phi$ reduces to ϕ_m sinc $((k+1) f_m \tau)$. Neglecting multiple reflections (take $k = 0$ term only) this results in a system frequency response identical to the one given by Kolner *et al.* [2] due to a single optical transit time. With nonuniform field it follows that the single transit time results in a system frequency response given by the Fourier transform of the field distribution, $\hat{H}_0 \phi(t) = \mathrm{Re} \{ v_g \int_0^{\tau} dt' \Delta k_m(v_g t') e^{i\omega_m t'} e^{-i\omega_m(t-\tau)} \}$.

C. Interferometric Effects

First, lets look at a case where the laser pulses are long compared to the substrate transit time. For the case of 100 μm thick GaAs substrate this corresponds to pulses longer than about 2.3 ps. We can then neglect the operator nature of $\hat{\phi}_0$ operating on the $E(t)$. We can furthermore assume that the phase perturbation $\phi(t)$ is slow compared to the transit time. Any time variation of $\phi(t)$ that is much faster than the sampling pulses will be lost in the sampling process anyway. With these assumptions we can set

$$\hat{H}_k \approx 1, \quad \hat{\phi}_0 \approx \phi_0 \tag{19}$$

and it immediately follows from (14) that $\hat{r}_j$ is a function of $(\phi_0 + \phi_j(t))$ only

$$\hat{r}_j = r(\phi_0 + \phi_j(t)) \tag{20}$$

where $r(\phi_0)$ is the amplitude reflection coefficient of the substrate etalon and is given by

$$r(\phi_0) \equiv |r(\phi_0)| \exp\{-i\Phi(\phi_0)\} = \frac{-r_f + r_b e^{-i\phi_0}}{1 - r_f r_b e^{-i\phi_0}}. \tag{21}$$

As expected, the substrate acts as an etalon with the round-trip phase "slowly" varying with the applied microwave field. From (3) (or (16)) the time averaged intensity can now be written as

$$\langle I_o(t) \rangle = \tfrac{1}{4} \langle | r(\phi_0 + \phi_x) - ir(\phi_0 + \phi_y) |^2 I(t) \rangle. \tag{22}$$

To evaluate the time average in the receiver, we expand $r(\phi_0 + \phi_j(t))$ in powers of $\phi_j(t)$. Usually $\phi_j(t)$ is very small, with circuit voltages $V(t)$ of the order of volts and half-wave voltages V_π of typical substrate materials of several kilovolts. We are then justified in taking only the first linear term in the expansion. Writing $\partial_{\phi_0} r/r = \partial_{\phi_0} \ln |r| - i \partial_{\phi_0} \Phi$, we have

$$\langle I_o(t) \rangle = \tfrac{1}{2} |r(\phi_0)|^2 \{ \langle I(t) \rangle - \partial_{\phi_0} \Phi \langle (\phi_y - \phi_x) \cdot I(t) \rangle - \partial_{\phi_0} \ln |r| \langle (\phi_x + \phi_y) I(t) \rangle \}. \tag{23}$$

Compared to (5), where we neglected etalon effects, there is an overall weighting factor $|r(\phi_0)|^2$ accounting for the reduced total reflected power. The second term in (23) is similar to the last term in (5), but with a new proportionality constant $\partial_{\phi_0} \Phi$. This is the normalized photon life time, τ_s/τ, of the substrate etalon, accounting for the changed effective optical transit time. Finally, we have a new term proportional to $\partial_{\phi_0} \ln |r|$. This term is due to a direct amplitude modulation in substrate due to interference at the top surface [8].

In GaAs substrates we have $\phi_x + \phi_y = 0$, and the last term in (23) would not contribute to the receiver signal. However, with a slight change of the set-up the intensity in the two polarizations would not be equal, and this term would contribute. Li *et al.* [8] demonstrated that one could use this direct amplitude modulation in the substrate to detect the electrooptic effect in GaAs microstrip lines without the use of an analyzing polarizer. With both polarizations incident on the substrate, the receiver signal (no polarizing beamsplitter) would be proportional to

$$\langle I_o(t)\rangle = |r|^2\{\langle I_x + I_y\rangle - 2\,\partial_{\phi_0} \ln |r|\,\langle \phi_x I_x + \phi_y I_y\rangle\} \tag{24}$$

Clearly if the magnitude of the reflection coefficient has a round trip phase dependence, the electrooptic signal will be nonzero. The receiver signal would show a strong input polarization dependence [8].

From (23) it follows that there are two calibration factors of interest for the direct electrooptic sampling set-up using long sampling pulses; $|r|^2\,\partial_{\phi_0} \ln |r|$ and $|r|^2\,\partial_{\phi_0}\Phi$. The phase derivatives follow from (21) as

$$\frac{\partial_{\phi_0} r(\phi_0)}{r(\phi_0)} = \frac{-ir_b(1 - r_f^2)}{(1 - r_f r_b e^{-i\phi_0})(r_b - r_f e^{i\phi_0})} \tag{25}$$

The resulting calibration factors are shown in Fig. 3(a) and (b) for GaAs substrates with constant front surface reflection coefficient and various back surface reflection coefficients. The electrooptic signal shows a resonant behavior as a function of the round-trip phase delay ϕ_0. The first calibration factor, $|r|^2\,\partial_{\phi_0}\Phi$, shown in Fig. 3(a), results in a large enhancement for the Gires–Tournois etalon for round-trip phases of $2n\pi$ (on resonance). For the symmetric etalon on the other hand, this calibration factor goes to zero on resonance. The other calibration factor, $|r|^2\,\partial\phi_0 \ln |r|$, shown in Fig. 3(b), is zero for the Gires–Tournois etalon. But only small deviations of the backside reflectivity from one, increases the calibration factor to a larger value (≈ 0.2) slightly off resonance.

Simple analytical expressions for the calibration factors can be derived in two special cases of interest. First is the Gires–Tournois etalon with $r_b = 1$, corresponding to the sampling geometries shown in Fig. 1(a) and (b). With a purely dispersive reflection coefficient only the first calibration factor, the normalized photon lifetime, is nonzero. The maximum and minimum normalized photon lifetime is given by $(1 + r_f)/(1 - r_f)$ and $(1 - r_f)/(1 + r_f)$, resulting in a maximum relative electrooptic signal variation of $\tau_{s,\max}/\tau_{s,min} = [(1 + r_f)/(1 - r_f)]^2$. For GaAs substrates this factor is approximately 13, resulting in a total electrooptic signal variation of 22 dB. The sensitivity to variations in ϕ_0 can be characterized by the finesse the resonance in Fig. 3(a). With $r_b = 1$ the finesse is given by $F = \pi\sqrt{r_f}/(1 - r_f)$ ($F \approx 5.4$ for GaAs).

The other case of interest is the symmetric Fabry–Perot etalon with $r_f = r_b$, corresponding to the sampling geometry in Fig. 1(c). For this geometry, we will in general have contributions from both terms in (23) if $\phi_x + \phi_y \neq 0$ or if the intensity in the two polarizations are not equal. The sensitivity is strongly reduced compared to the enhanced sensitivity for the Gires–Tournois etalon. Off resonance, the calibration factor shown in Fig. 3(a) is approximately $2r_f^2(1 - r_f^2)/(1 + r_f^2)^3$ (0.19 or −14.5 dB for GaAs). For the set-up considered in this paper ($I_x = I_y$), the sensitivity goes to zero on resonance.

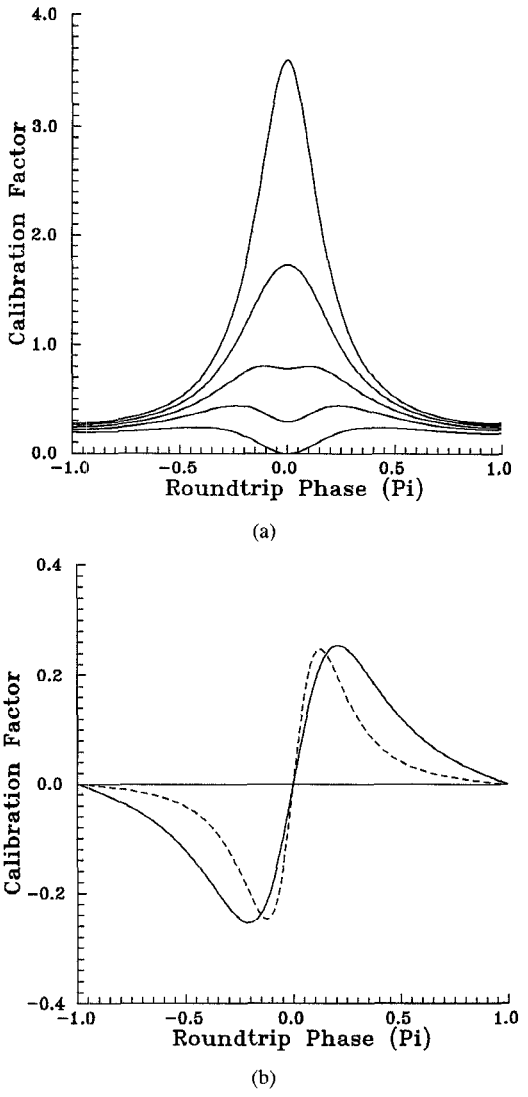

Fig. 3. Calibration factors as function of round trip phase delay for GaAs substrates with front surface reflection coefficient $r_f = 0.565$ and various back surface reflection coefficient r_b. (a) $|r|^2\,\partial_{\phi_0}\Phi$. $r_b = 1.0, 0.9, 0.8, 0.7$, and 0.565. The upper trace corresponds to a Gires–Tournois etalon with $r_b = 1.0$, and the lower trace corresponds to a symmetric Fabry–Perot etalon with $r_f = r_b = 0.565$. (b) $|r|^2\,\partial_{\phi_0} \ln |r|$. $r_b = 1.0$ horizontal solid line, $r_b = 0.9$ dotted line, and $r_b = 0.565$ solid line.

The calibration factors considered here are all periodic functions of the round trip phase ϕ_0, making them periodic in both probe wavelength and substrate thickness. For a fixed probe wavelength, a substrate thickness variation of $\lambda/2n$, or 0.14 μm in GaAs at 1 μm probe wavelength, is enough to change the signal from maximum to minimum. To get an idea of how severe this requirement is, consider a 2 inch GaAs wafer. A maximum thickness variation of less than $\lambda/2n$ across the wafer would require the two surfaces to be parallel within about $3 * 10^{-6}$ ra-

dians. Typically a MMIC would not cover the entire wafer, but even a circuit of dimensions less than a centimeter would likely show thickness variations larger than $\lambda/2n$.

In the calculation of the interferometric effects above, we assumed that the laser pulses were coherent or transform limited. For a Nd:YAG laser, this is a reasonable approximation. For a dye laser, one can have considerable wavelength chirp in addition to both amplitude and phase noise. This would reduce the finesse of the resonance somewhat. However, it would still contribute a large calibration factor. To avoid any interferometric effects, the laser line would have to be broader than the free spectral range of the etalon. For a 100 μm GaAs substrate, this corresponds to a line broader than 430 GHz or 1.4 nm, which is broader than most modelocked with pulse widths much larger than the substrate transit time.

D. Multiple Reflection Effects

Now consider probing with very short laser pulses, pulses shorter than the substrate transit time. Such short pulses can easily be achieved using commercially available subpicosecond modelocked laser systems, even for substrate thicknesses of less than 100 μm. The temporal response of the sampling system is then usually assumed to be limited by the substrate transit time [1], [2]. As we discussed in Section II-B multiple reflections in the substrate would increase the effective transit time, and therefore further reduce the system bandwidth.

For the short pulses considered here one can neglect interference between the reflected pulses at the boundaries of the substrate. Neglecting interference, (16) can be written

$$\langle I_o(t)\rangle = \tfrac{1}{2}\Big\{ R_f\langle I(t)\rangle + \tfrac{1}{2}R_b T_f^2 \sum_{k=0}^{\infty} (R_f R_b)^k \cdot \langle | e^{-i(k+1)\hat{H}_k\phi_x} - ie^{-i(k+1)\hat{H}_k\phi_y}|^2 \cdot e^{-(k+1)\tau\partial_t} I(t)\rangle \Big\} \tag{26}$$

where $R_f = |r_f|^2$, $R_b = |r_b|^2$, and $T_f = |t_f|^2$. Assuming $(k+1)\hat{H}_k\phi_j \ll \pi/2$, we can write (26) in the form

$$\langle I_o(t)\rangle = \frac{1}{2}\Big\{ R_f\langle I(t)\rangle + \frac{R_b T_f^2}{1 - R_f R_b} \cdot \Big[\langle I(t)\rangle - (1 - R_f R_b)\sum_{k=0}^{\infty}(k+1) \cdot (R_f R_b)^k \langle \hat{H}_k(\phi_x - \phi_y) e^{-(k+1)\tau\partial_t} I(t)\rangle\Big]\Big\}. \tag{27}$$

The first term in the curly braces is the direct reflection from the top surface. Apart from this term and the overall scaling factor $R_b T_f^2/(1 - R_f R_b)$, the last two terms look similar to the case neglecting multiple reflections. The successive reflections sample a filtered version of the microwave field $(\hat{H}_k\phi)$ each weighted by $(1 - R_f R_b)(R_f R_b)^k$.

To find an expression for the time averaged output intensity for a sinusoidal microwave field excitation, we use (17) for $\hat{H}_k\phi(t)$. Furthermore, we use the approximation $\exp(ik\Delta\omega\tau) \approx 1$. With an IF frequency $\Delta\omega$ typically very low compared to the microwave frequency ω_m (from a few hertz up to about 10 MHz) this approximation should always be good. With this and (6) we find

$$\langle I_o(t)\rangle = \frac{1}{2}\langle I(t)\rangle \Big\{ R_f + \frac{R_b T_f^2}{1 - R_f R_b}\Big[1 - N(\omega_m)\frac{2\pi}{V_\pi}|\hat{V}| \cdot \cos(\Delta\omega t + \phi_V + \omega_m\tau/2 + \Theta_N(\omega_m))\Big]\Big\}. \tag{28}$$

where we have defined

$$N(\omega_m) = g(\omega_m)\frac{\sin(\omega_m\tau/2)}{\omega_m\tau/2}\frac{1}{(1 - R_f R_b)} \cdot \frac{1}{\sqrt{1 + \dfrac{4R_f R_b}{(1 - R_f R_b)^2}\sin^2\dfrac{\omega_m\tau}{2}}} \tag{29}$$

$$\Theta_N(\omega_m) = \tan^{-1}\left[\frac{2R_f R_b}{1 - R_f R_b}\frac{\sin\dfrac{\omega_m\tau}{2}\cos\dfrac{\omega_m\tau}{2}}{1 + \dfrac{2R_f R_b}{1 - R_f R_b}\sin^2\dfrac{\omega_m\tau}{2}}\right] \tag{30}$$

and $g(\omega_m)$ is defined in (18). The system sensitivity is reduced by an amplitude calibration factor $N(\omega_m)R_b T_f^2/(1 - R_f R_b)$ as shown in Fig. 4(a). In the figure we have assumed a uniform microwave field and set $g(\omega_m) = 1$. Also plotted is the single transit time system frequency response $\sin(\omega_m\tau/2)/(\omega_m\tau/2)$. It is interesting to note that for the Gires–Tournois etalon ($R_b = 1$), the reduction of the sensitivity due to the first front surface reflection is exactly compensated by the enhancement due to the multiple reflections in the substrate, resulting in a calibration factor of one in the low-frequency limit. For higher frequencies, multiple reflections results in a significant reduction in sensitivity. For a 100 μm GaAs substrate the 3 dB bandwidth is reduced to about 80 GHz as compared to 190 GHz for the single transit time approximation. We should note that the multiple reflection effects (bandwidth limitations) an put quite restrictive bandwidth limitations in the back-side probing on coplanar strip lines. The thick substrate often used with these transmission lines could increase the substrate transit time significantly, to show significant effects already at 40 GHz. This is, of course, under the assumption of a good quality surface (which is by the way desirable for all optical probing experiments). Tighter focusing of the probe beam would reduce the re-

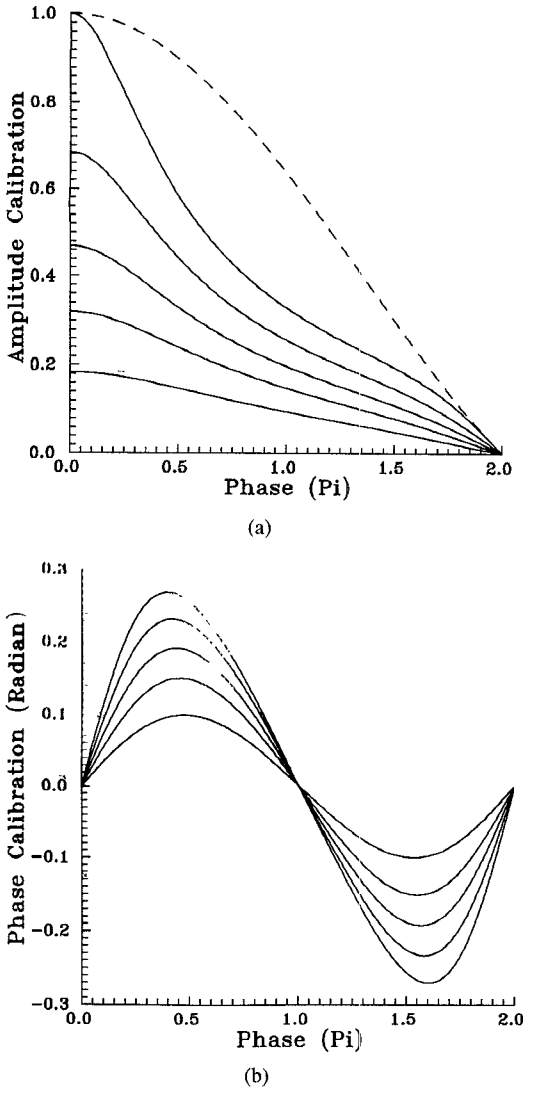

Fig. 4. Calibration factors as a function of $\omega_m \tau$ for GaAs substrates with front surface reflection coefficient $r_f = 0.565$ and various back surface reflection coefficients $r_b = 1.0$, 0.9, 0.8, 0.7, and 0.565. (a) Amplitude calibration factor. The upper trace (solid line) corresponds to a Gires–Tournois etalon with $r_b = 1.0$, and the lower trace corresponds to a symmetric Fabry–Perot etalon with $r_f = r_b = 0.565$. Dashed line shows single transit time system frequency response. (b) Phase calibration factor. The Gires–Tournois ($r_b = 1$) shows the largest phase factor while the symmetric Fabry–Perot etalon show the smallest phase factor.

ceived power of the multiple delayed pulses and therefore reduce the effect on the measurement system bandwidth. For the symmetric Fabry–Perot etalon, the frequency dependence of the amplitude calibration factor is negligible, but the sensitivity is reduced by a factor $R_b(1 - R_f)^2/(1 - R_f R_b)^2$, corresponding to a factor of 5 (or 14 dB) in GaAs.

The linear phase shift $\omega_m \tau/2$ in (28) corresponds to a time shift and is not important. The other phase factor $\Theta_N(\omega_m)$ is not linear and would affect the system pulse response. Fig. 4(b) shows $\Theta_N(\omega_m)$ for various etalon parameters. The Gires–Tournois etalon shows the strongest frequency dependence with a maximum phase deviation of about 15 degrees. The symmetric Fabry–Perot etalon shows a maximum phase deviation of about 6 degrees. For low frequencies Θ_N is linear and the different slopes correspond to different time delays. It follows from Fig. 4 that for signals with frequency components such that $f > 1/6\tau$ would be significantly distorted in the sampling system. This corresponds to about 70 GHz in a typical microstrip circuit.

E. Geometric Calibration Factors

As shown in the previous section the electrooptic signal is directly proportional to the potential difference between the front and back surface of the substrate at the probe position. This potential difference will have contribution from all surrounding signal lines. Assuming the sensitivity reduction/enhancement due to etalon effects are known, the measured electrooptic signal can be related to the voltage at the test point by modeling the potential distributions around the signal lines. Various groups have used numerical techniques to calculate the potential distribution in some typical geometries [9]–[11], [6]. However, to easily calibrate these vibrations out of the measurement simple analytical correction factors are needed. Usually, the major contribution to the electrooptic signal will be due to the line closest to the probe beam position, and all one has to consider is the potential distribution close to a single conductor. Here we concentrate on the specific case of a microstrip line, and calculate a voltage calibration factor as a function of the transverse position of the probe beam.

The field on a typical microstrip line is well confined to the area close to the conducting strip, causing the surface potential to drop off rapidly as we move out from the conductor edge. Close to the edge, the normal field is reasonably approximated by the field from a semi-infinite patch. That is, we have an inverse square root singularity of the normal field at the edge. The approximate surface potential can be found by integrating the normal field along the surface

$$V(x) = V_0 \left\{ 1 - \frac{2}{\sqrt{\pi}} \sqrt{\frac{\epsilon}{1 + \epsilon}} \sqrt{\frac{x}{h}} \right\} \tag{31}$$

where V_0 is the line potential, and ϵ is the substrate relative dielectric constant. This approximate form for the surface potential is good for $x/h < 1/2$ for high ϵ substrates, and to even larger x/h for low ϵ substrates. The exact solution for the static potential drops somewhat faster than what is indicated by (31) for large x/h [6]. The measured voltage at probe position x_0 using an optical probe beam with transverse intensity variation $I(x)$ is given by

$$V_m(x_0) = \int_0^\infty dx\, V(x)\, I(x) \tag{32}$$

where we have neglected any proportionality factors due to the etalon effects discussed in the previous sections. Furthermore, we neglect the changing beam waist away from the focus, which have been shown to only slightly

modify the electrooptic signal [9]. The intensity distribution can be approximated by a Gaussian beam with Gaussian spot size ω_0, positioned a distance x_0 from the conductor edge, $I(x) = 2I_0/(\omega_0\sqrt{2\pi})\exp\{-2(x - x_0)^2/w_0^2\}$. To keep the probe diameter approximately constant throughout the substrate one should choose the Rayleigh range of the probe beam, $z_R = \pi\omega_0^2 n/\lambda$, approximately equal to or longer than the substrate thickness (corresponding to $\omega_0 > 3$ μm for a 100 μm GaAs substrate). We then have

$$V_m(x_0) = V_0\left\{\frac{1}{\sqrt{2\pi}}\int_0^\infty ds e^{-(1/2)(s-2x_0/w_0)^2} - \frac{2}{\sqrt{\pi}}\sqrt{\frac{\epsilon}{1+\epsilon}}\sqrt{\frac{w_0}{2h}}\frac{1}{\sqrt{2\pi}}\int_0^\infty ds\sqrt{s} \cdot e^{-(1/2)(s-2x_0/w_0)^2}\right\} \quad (33)$$

The calibration factor V_m/V_0 is shown in Fig. 5 for the case of a microstrip line on a GaAs substrate with $\epsilon = 12.5$. It is clear from Fig. 5 that the electrooptic signal is maximum when $x_0 \approx w_0$, and it is decreasing to either side of this "optimum" position. Moving closer to the electrode blocks part of the beam causing the signal to drop rapidly. To avoid diffraction from the conductor edge, one wants $x_0 \geq w_0$, such that (33) can be approximated as

$$V_m(x_0) = V_0\left\{1 - \frac{2}{\sqrt{\pi}}\sqrt{\frac{\epsilon}{1+\epsilon}}\sqrt{\frac{x_0}{h}}\right\}. \quad (34)$$

For $x_0 \geq w_0$ the error in this approximation is less than about 2% as compared to (33). Typically, to maximize the signal one would use $x_0 \approx w_0$, and therefore, the calibration factor decreases with the square root of the spot size. For a 100 μm thick GaAs substrate this leads to a 4 dB signal reductions for a 10 μm spot size and a 8 dB signal reduction for a 30 μm spot size. It is interesting to note that even large spot sizes, the measured potential distribution $V_m(x_0)$ is to a good approximation equal to the actual potential distribution $V(x_0)$ for $x_0 > w_0$.

III. Experimental Verification

To verify some of the theoretical results presented in the previous sections, we have used an electrooptic sampling set-up to measure the electrooptic signal variation as a function of both spatial position and of probe wavelength. A simplified schematic of the experimental set-up is shown in Fig. 6. The circuit used was a 4–6 GHz GaAs MMIC amplifier using microstrip lines on 100 μm substrate (courtesy of General Electric). The laser sources used were a modelocked Nd : YAG laser operating at 1064 nm with nominally 90 ps pulses, and a tunable synchronously pumped modelocked dye laser tunable from 900–980 nm (Styryl-13 dye) with approximately 8 ps pulses. The measurements were taken at a fixed microwave frequency of 5 GHz. The probe beam was focused to a 10 μm spot size and the probe position could be scanned along the microstrip line using stepper motors.

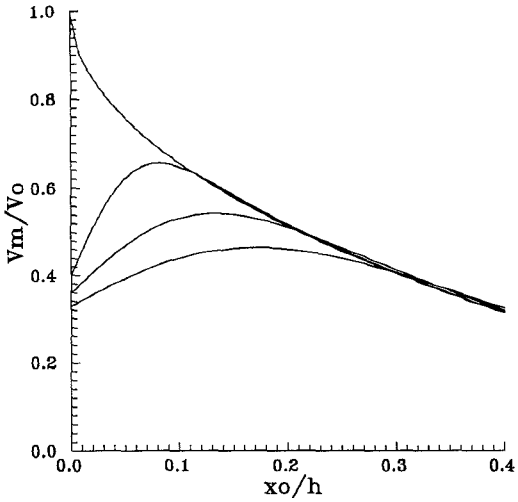

Fig. 5. Voltage calibration factor for a microstrip on a GaAs substrate as a function of probe position x_0 relative to the microstrip line edge for probe beam diameters of 0 * h, 0.1 * h, 0.2 * h, and 0.3 * h.

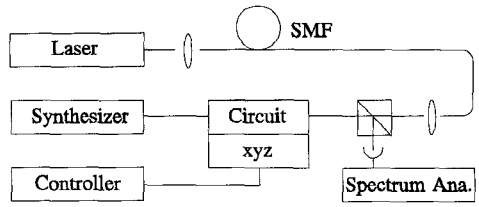

Fig. 6. A simplified schematic of the experimental set-up. The sampling pulses were coupled to the electrooptic sampling head through a polarization preserving single mode fiber (SMF). The circuit under test is mounted on a stepper-motor controlled micropositioning stage (xyz).

Fig. 7 shows the measured electrooptic signal variation along the microstrip line. The data shows a resonant behavior in agreement with the discussion in Section II-B. The maximum signal variation is approximately 22 dB in excellent agreement with the predictions assuming $r_b = 1$ and $r_f = 0.565$. The period of the variations is 80–90 μm, corresponding to local thickness variations corresponding to an angle of only slightly more than a milliradian (0.0017 mrad). The slow decay of the electrooptic signal as a function of position is due to taking a scan not quite parallel to the microstrip line. This variation can be accounted for by the position dependent calibration factor discussed in Section II-C. Similar observations have recently been reported by Li *et al.* [8] using a 15 ps Nd : YAG laser pulse on a 320 μm GaAs substrate (approximately 7 ps round trip time).

In Fig. 8 we show the result using the dye laser at a wavelength of about 965 nm. Two different probe wavelengths were used, separated by about 1 nm. The measurements were performed by adjusting the birefringent tuner in the laser without touching the circuit or sampling

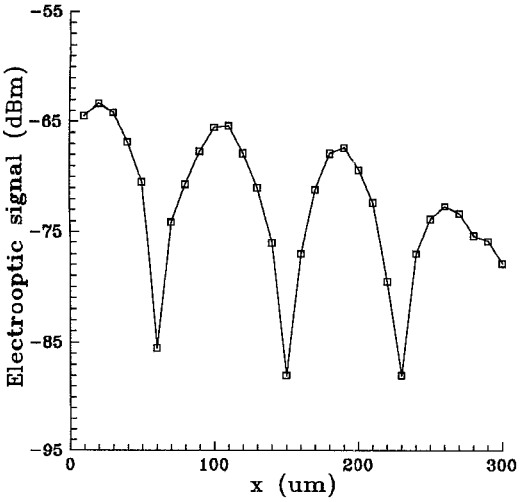

Fig. 7. Measured electrooptic signal variation as a function of the spatial coordinate parallel to the microstrip line on a 100 μm thick GaAs substrate. The laser source used was a Nd:YAG laser operating at 1.064 μm with $\tau_p \approx 90$ ps.

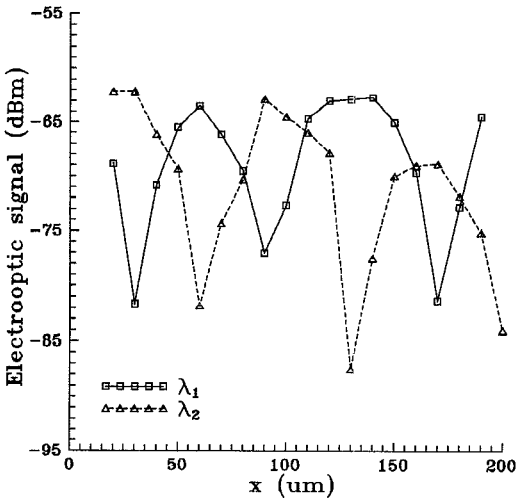

Fig. 8. Same as in Fig. 7, but measured using two different dye laser wavelengths separated by about 1 nm at 965 nm. $\tau_p \approx 8$ ps.

head. Therefore, the shift of the fringes in Fig. 8 is solely due to the probe wavelength shift. Due to the coarse wavelength tuning of the laser, it was not possible to do a continuous tuning of the probe wavelength over one etalon free spectral range (≈ 1.4 nm). Even without this continuous tuning, the half-period shift of the fringe pattern supports the conjecture that the resonant behavior is due to interferometric effects. The slightly noisier fringes measured with the dye laser as compared to the Nd:YAG laser is due the stronger amplitude noise for the dye laser.

Due to the limitation in microwave equipment, we did not try to verify the bandwidth limitations due to the multiple reflection effects discussed in Section II-D.

IV. Deembedding and Calibration

It is clear from the previous sections that the direct electrooptic sampling system can introduce significant measurement errors that must be removed if accurate measurements are to be made. Various deembedding procedures to implement the calibration can be designed using our model of the sampling system. The most difficult problem in calibrating the system comes from the interferometric effects discussed in Section II-C. The multiple reflection effects in the short pulse limit (Section II-D) only shows a weak dependence on the substrate thickness and very small uncertainties would result from the substrate thickness variations. The most severe problem in this case would be reflectivity variations across the circuit. For well prepared circuits this variation is likely to be small, only a few percent. The interferometric effects, on the other hand, shows extreme sensitivity to substrate thickness variations and cannot be controlled or corrected for without a deembedding algorithm. The geometric factors discussed in Section II-E can be corrected for if one has accurate measurement of the position of the probe beam relative to the conductors.

There are several techniques to deembed the etalon effects in the long pulse limit. One technique is to make the measurement at two (or more) different (known) wavelengths. This would require a precisely tunable laser wavelength. It would then be possible to remove the interferometric effects via calibration software using etalon theory. This is possible since the average detector power is affected by the etalon effective reflectivity only, while the electrooptic signal is affected by both the etalon storage time and effective reflectivity. An alternative technique is possible if the effective reflectivities of the surfaces of the etalon are both considerably less than one. (We have found this to be the case for most circuits due to large absorption in the Ti bonding layer used for Ti/Au electrodes on standard MMICs.) Since the variation of the substrate thickness as a function of spatial position directly effects the average detector power, this can be used to infer the total effective round trip phase delays induced by the etalon. From the spatial variation and overall contrast of the average detector signal, both the average backside reflectivity and the local phase delay can be obtained. From this the reflectivity/storage time correction for the electrooptic signal can be computed and used to deembed the etalon effects from the electrooptic signal. In preliminary tests, we have used this technique to produce significant improvements of one dimensional spatial scans on microstrip circuits. However, a number of issues have to be resolved before a general deembedding procedure for spatial scans can be developed. This includes the effect of fine scale surface roughness, and the extent of local variations of the backside reflectivity in typical MMICs.

V. Conclusion

In reflection mode optical probing, the circuit substrate forms an etalon for optical probe beam. In this paper we have presented results showing the effect of this etalon on the voltage calibration factor of the electrooptic sampling system. Analytical expressions for the calibration factors are derived in two limiting cases; long and short optical

sampling pulses. Depending on the length of the sampling pulse relative to the substrate transit time, the etalon will affect either the voltage calibration factor or the system bandwidth. For pulses long compared to the transit time, interference at the surface results in a probe wavelength dependent storage time effect. The resulting electrooptic signal shows a resonant behavior as a function of wavelength or substrate thickness. For probing in microstrip circuits on GaAs substrates this could result in a maximum signal variation of 22 dB. By using pulses short compared to the substrate transit time, these interferometric effects can be eliminated. In this case the multiple reflections reduce the effective system bandwidth to a bandwidth less than that given by the transit time or by the sampling pulse width. Amplitude and phase calibration factors are derived. For probing on a microstrip line on a 100 μm GaAs substrate, the 3 dB bandwidth is reduced to about 80 GHz, with even larger bandwidth reductions for thicker substrates.

The decaying surface potential close to a microstrip line results in a voltage calibration factor that reduces the sensitivity of the sampling system proportional to the square root of the probe beam spot size. The resulting electrooptic signal reduction is 4 dB for a 10 μm spot and 8 dB for a 30 μm spot on 100 μm thick GaAs substrates.

Various deembedding procedures to implement the calibration of the direct electrooptic sampling system can be designed using our model of the sampling system. Two possible procedures based on wavelength tuning and spatial scanning were discussed.

Although we have limited our discussion to reflection mode probing in typical microwave transmission lines, it should be clear that the effects discussed here would similarly be seen in transmission mode sampling, only differing by the exact form of the calibration factors.

Acknowledgment

The authors are grateful to one of the reviewers for drawing their attention to the recent work of Li *et al.* [8].

References

[1] J. A. Valdmanis and G. Mourou, "Sub-picosecond electro-optic sampling: Principles and applications," *IEEE J. Quantum Electron.*, vol. QE-22, pp. 69–78, 1986.

[2] B. H. Kolner and D. M. Bloom, "Electrooptic sampling in GaAs integrated circuits," *IEEE J. Quantum Electron.*, vol. QE-22, pp. 79–93, 1986.

[3] K. J. Weingarten, M. J. Rodwell, and D. M. Bloom, "Picosecond optical sampling of GaAs integrated circuits," *IEEE J. Quantum Electron.*, vol. QE-24, pp. 198–220, 1988.

[4] J. M. Wiesenfeld, "Electro-optic sampling of high-speed devices and integrated circuits," *IBM J. Res. Develop.*, vol. 34, pp. 141–161, 1990.

[5] J. A. Valdmanis, "Electro-optic measurement techniques for picosecond materials, devices, and integrated circuits," ch. 4 in *Measurement of High-Speed Signals in Solid State Devices, Semiconductors and Semimetals*, vol. 28, Vol. Ed. R. B. Marcuse, Boston: Academic Press, 1990.

[6] J. M. Wiesenfeld and R. K. Jain, "Direct optical probing of integrated circuits and high-speed devices," ch. 5 in *Measurements of High-Speed Signals in Solid State Devices, Semiconductors and Semimetals*, vol. 28, Vol. Ed. R. B. Marcuse, Boston: Academic Press, 1990.

[7] E. W. Strid, "26 GHz wafer probing for MMIC development and manufacture," *Microwave J.*, vol. 29, pp. 71–82, 1986.

[8] M. G. Li, E. A. Chauchard, C. H. Lee, and H.-L. A. Hung, "Microwave modulation of optical signal by electro-optic effect in GaAs microstrip," in *1990 IEEE MTT-S Int. Microwave Symp. Dig.*, 1990, pp. 945–948.

[9] J. L. Freeman, S. R. Jefferies, and B. A. Auld, "Full-field modeling of the longitudinal electro-optic probe," *Opt. Lett.*, 12, pp. 795–797, 1987.

[10] J. L. Freeman, D. M. Bloom, S. R. Jefferies, and B. A. Auld, "Accuracy of electro-optic measurements of coplanar waveguide transmission lines," *Appl. Phys. Lett.*, 53, pp. 7–9, 1988.

[11] ——, "Sensitivity of direct electro-optic sampling to adjacent signal lines," *Appl. Phys. Lett.*, vol. 54, pp. 478–480, 1989.

[12] F. Gires and P. Tournois, "An interferometer useful for pulse compression of a frequency modulated light pulse," *C. R. Acad. Sci.*, Paris, vol. 258, pp. 6112–6115, 1964.

[13] D. R. Hjelme and A. R. Mickelson, "Gain nonlinearities due to carrier density dependent dispersion in semiconductor lasers," *IEEE J. Quantum Electron.*, vol. 21, pp. 443–451, 1989.

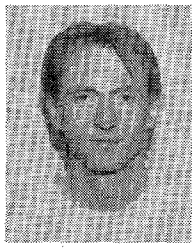

Dag Roar Hjelme was born in Valldal, Norway, on March 25, 1959. He received the M.S. degree in electrical engineering from the Norwegian Institute of Technology, Trondheim, Norway, in 1982, and the Ph.D. degree in electrical engineering from the University of Colorado, Boulder, in 1988.

From 1983 to 1984 he was with the Norwegian Institute of Technology, Division of Physical Electronics, working on fiber optics and integrated optics. He is currently a Postdoctoral Research Associate with the Department of Electrical Engineering, University of Colorado. His current research interests include the dynamic and spectral properties of semiconductor lasers, microwave optics, and optoelectronics.

Alan Rolf Mickelson was born in Westport, CT, on May 2, 1950. He received the B.S.E.E. degree from the University of Texas, El Paso, in 1973, and the M.S. and Ph.D. degrees from the California Institute of Technology, Pasadena, in 1974 and 1978, respectively.

Following a postdoctoral period at Caltech in 1980, he joined the Electronics Research Laboratory of the Norwegian Institute of Technology, Trondheim, Norway, at first as an NTNF Postdoctoral Fellow, and later as a staff scientist. His research in Norway primarily concerned characterization of optical fibers and fiber compatible components and devices. In 1984 he joined the Department of Electrical and Computer Engineering at the University of Colorado, Boulder, where he became an Associate Professor in 1986. His research presently involves semiconductor laser characterization, integrated optic device fabrication and characterization, and fiber system characterization.